bolometer; photon, phonon, Johnson, and readout (from both cold and warm readout electronics). To validate our calculations, we compared two independent software packages that have been validated with several operating CMB instruments. The calculations agreed within 1% both for individual noise terms and for overall mission noise. A detailed description of the PICO noise model and its inputs is available in Young et al. [247]; small differences between that publication and Table 3.2 are due to refinements of the primary mirror and stop temperatures.

Laboratory experiments have demonstrated that TES bolometers can be made background-limited in the low loading environment they would experience at L2 [257]. For PICO, the primary contributor to noise is the optical load. The sources of optical load are the CMB, reflectors, aperture stop, and low-pass filters. The CMB and stop account for at least 50% of the optical load at all frequencies up to and including 555 GHz. At higher bands emission from the primary mirror dominates.

The sensitivity model assumes white noise at all frequencies. Sub-orbital submillimeter experiments have demonstrated TES detectors that are stable to at least as low as 20 mHz [258], meeting the requirements for PICO's scan strategy (§ 4.1.2).

## 3.3 Detector Readout

Suborbital experiment teams over the past ten years have chosen to use voltage-biased TESs because their current readout scheme lends itself to Superconducting Quantum Interface Device (SQUID) based multiplexing. Multiplexing reduces the number of wires to the cryogenic stages and thus the total thermal load that the cryocoolers must dissipate. This approach also simplifies the instrument design.

In the multiplexing circuitry, SQUIDs function as low-noise amplifiers and cryogenic switches. The current baseline for PICO is to use a time-domain multiplexer (TDM), which assigns each detector's address in a square matrix of simultaneously read columns, and sequentially cycles through each row of the array [259]. The PICO baseline architecture uses a matrix of 128 rows and 102 columns. The thermal loading on the cold stages from the wire harnesses is subdominant to conductive loading through the mechanical support structures.

Because SQUIDs are sensitive magnetometers, suborbital experiments have developed techniques to shield them from Earth's magnetic field using highly permeable materials and superconducting materials [260]. Total suppression factors better than $10^7$ have been demonstrated for dynamic magnetic fields [261]. PICO will use these demonstrated techniques to shield SQUID readout chips from the ambient magnetic environment, which is 20,000 times smaller than near Earth, as well as from fields generated by on-board components, including the cADR (§ 3.4.1). The cADR is delivered with its own magnetic shielding, which reduces the field to less than 0.1 G (less than that experienced by suborbital experiments).

SQUIDS are also sensitive to radio-frequency interference (RFI). Several suborbital experiments have demonstrated RFI shielding using aluminized mylar wrapped at cryogenic stages to form a Faraday cage around the SQUIDs [262–264]. Cable shielding extends the Faraday cage to the detector warm readout electronics.

Redundant warm electronics boxes perform detector readout and instrument housekeeping using commercially available radiation-hardened analog-to-digital converters (ADCs), requiring 75 W total. The readout electronics compress the data before delivering them to the spacecraft, requiring an additional 15 W. PICO detectors produce a total of 6.1 Tbits/day assuming 16 bits/sample, sampling rates from Table 3.1, and bolometer counts from Table 3.2. *Planck* HFI typically achieved 4.7× compression in flight, with information loss increasing noise by ~10% [265, 266]. Suborbital work has demonstrated 6.2× lossless compression [267]. PICO assumes 4× lossless compression.

## 3.4 Thermal

Like the *Planck*-HFI instrument, PICO's focal plane is maintained at 0.1 K to ensure low detector noise while implementing a readily available technology (§ 3.4.1). To minimize detector noise due to instrument

Table 3.3: Projected cooler heat lift capabilities offer more than 100% heat lift margin, complying with cooler technology best practices [268].

| Component | Temperature [K] | | Active Heat Lift [mW] | | |
|---|---|---|---|---|---|
| | Required | CBE | Required per model[a] | Capability today | Projected capability |
| Primary reflector | < 40 | 17 | N/A (radiatively cooled) | | |
| Secondary reflector | < 8 | 4.5 | 42 at 4.5 K | > 55 at 6.2 K[b] | > 100 at 4.5 K[c] |
| Aperture stop | 4.5 | 4.5 | | | |
| cADR heat rejection[d] | 4.5 | 4.5 | | | |
| Focal plane enclosure and filter | 1.0 | 1.0 | 0.36 | 1.0 | N/A[e] |
| Focal plane | 0.1 | 0.1 | $5.7 \times 10^{-3}$ | $32 \times 10^{-3}$ | N/A[e] |

[a] The required loads were calculated using Thermal Desktop. Reference [269] was used to estimate the thermal conductive loads through mechanical supports. In addition to the listed components, the total 4.5 K heat load includes the intercept on the focal plane mechanical supports. [b] Reference [270]. [c] Both NGAS and Ball project > 100 mW lift capability at 4.5 K using higher compression-ratio compressors currently in development (§ 3.4.2 and Fig. 3.4). [d] The cADR lift capability at 1 K and 0.1 K is from a Goddard quote. [e] Capability today already exceeds requirement.

thermal radiation, the aperture stop and reflectors are cooled using both active and radiative cooling (§ 3.4.2, § 3.4.3, Fig. 3.2). All thermal requirements are met with robust margins (Table 3.3).

### 3.4.1 cADR Sub-Kelvin Cooling

A multi-stage continuous adiabatic demagnetization refrigerator (cADR) maintains the PICO focal plane at 0.1 K and the surrounding enclosure, filter, and readout components at 1 K. The cADR employs three refrigerant assemblies operating sequentially to absorb heat from the focal plane at 0.1 K and reject it to 1 K. Two additional assemblies, also operating sequentially, absorb this rejected heat at 1 K, cool other components to 1 K, and reject heat at 4.5 K. This configuration provides continuous cooling with small temperature variations at both the 0.1 K and 1 K. Heat straps connect the two cADR cold sinks to multiple points on the focal plane assembly, which has high thermal conductance paths built in, to provide spatial temperature uniformity and stability during operation. The detector arrays are thermally sunk to the mounting frame. Heat loads in the range of 30 $\mu$W at 0.1 K and 1 mW at 1 K (time-average) are within the capabilities of current cADRs developed by GSFC (§ 6.3) [271, 272]. The PICO sub-kelvin heat loads are estimated at less than half of this capability (Table 3.3).

### 3.4.2 4.5 K Cooler

A cryocooler system similar to that used on JWST to cool the MIRI detectors [273, 274] removes the heat rejected from the cADR and cools the aperture stop and secondary reflector to 4.5 K. Both NGAS (which provided the MIRI coolers) and Ball Aerospace have developed such coolers under the NASA-sponsored Advanced Cryocooler Technology Development Program [275]. NGAS and Ball use slightly different but functionally-equivalent hardware approaches. A 3-stage precooler provides 16 K precooling to a separate circulated-gas loop. The circulated-gas loop utilizes Joule–Thomson (J-T) expansion, further cooling the gas to 4.5 K. The J-T expansion point is located close to the cADR heat rejection point and provides it the lowest temperature. Subsequently, the gas flow intercepts heat conducted to the focal plane enclosure, then cools the aperture stop and the secondary reflector before returning to the circulation compressor.

NGAS and Ball are actively working on increasing the flow rate and compression ratio of the J-T compressor, which should result in higher system efficiency and greater heat-lift relative to the current MIRI cooler. NGAS uses $^4$He as the circulating gas, as was used for MIRI. Ball uses a somewhat larger compressor and $^3$He as the circulating gas. Both employ re-optimized heat exchangers. The NGAS project has completed PDR-level development, and is expected to reach CDR well before PICO begins Phase-A. The projected performance of this cooler is shown in Fig. 3.4; it gives 100 mW at 250 W input power, which

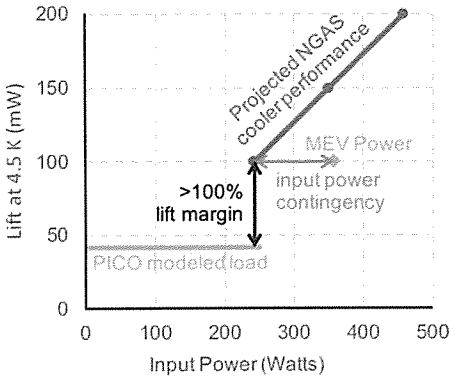


Figure 3.4: Projected performance of the NGAS cooler using a multi-stage compressor and $^4$He circulating gas [274] meets PICO's requirements with $> 100\,\%$ margin. PICO requires heat lift of 42 mW at 4.5 K (Table 3.3). With 250 W of input power the NGAS cooler is projected to provide 100 mW of heat lift. We conservatively specify a maximum expected value (MEV) of 350 W as the compressor's input power, giving 100 W of additional input power contingency.

is more than 100 % heat lift margin relative to PICO's requirements (Table 3.3). For PICO we assumed an input power of 350 W.

The entire precooler assembly and the J-T circulator compressor are located on the warm spacecraft spun module (Fig. 3.2). All waste heat rejected by the cooler compressors and drive electronics is transferred to the spacecraft heat rejection system. Unlike JWST, the PICO cooler does not require deployment of the remote cold head.

### 3.4.3 Radiative Cooling

A set of four V-groove radiators provides passive cooling. This is standard technology, with origins dating more than 30 years (§ 6.3). The outermost of the four V-groove shields shadows the interior shields from the Sun. The V-grooves radiate to space, each reaching successively cooler temperatures. The V-groove assembly provides a cold radiative environment to the primary reflector, structural ring, and telescope box, so radiative loads on those elements are smaller than the conductive loads through the mechanical support structures.

## 3.5 Instrument Integration and Test

PICO instrument I&T planning benefits greatly from heritage experience with the *Planck* HFI instrument [276].

PICO screens detector wafer performance prior to selection of flight wafers and focal plane integration. The cADR and 4 K cryocooler are qualified prior to delivery. The relative alignment of the two reflectors under thermal contraction is photogrammetrically verified in a thermal vacuum (TVAC) chamber.

PICO integrates the flight focal plane assembly and flight cADR in a dedicated sub-kelvin cryogenic testbed. Noise, responsivity, and focal-plane temperature stability are characterized using a representative optical load for each frequency band (temperature-controlled blackbody). Polarimetric and spectroscopic calibration are performed.

The focal plane is integrated with the reflectors and structures, and alignment verified photogrammetrically at cold temperatures in a TVAC chamber. The completely integrated observatory (instrument and spacecraft bus) is tested in TVAC to measure parasitic optical loading from the instrument, noise, microphonics, and radio-frequency interference (RFI). The observatory is 4.5 m in diameter and 6.1 m tall, with no deployables.

# 4 Design Reference Mission

The PICO design reference mission is summarized in Table 4.1.

## 4.1 Concept of Operations

The PICO concept of operations is similar to that of the successful *WMAP* [277] and *Planck* [278] missions. After launch, PICO cruises to a quasi-halo orbit around the Earth–Sun L2 Lagrange point (§ 4.1.1). A two-week decontamination period is followed by instrument cooldown, lasting about two months. After in-orbit checkout is complete, PICO begins the science survey.

Table 4.1: PICO carries margin on key mission parameters. Maximum Expected Value (MEV) includes contingency.

| | |
|---|---|
| Orbit type . . . . . | Sun-Earth L2 Quasi-Halo |
| Mission class . . . . . | Class B |
| Mission duration . . . . . | 5 years |
| Propellant (hydrazine) . . . | 213 kg (77 % tank fill) |
| Launch mass (MEV) . . . . | 2147 kg (3195 kg capability) |
| Max power (MEV) . . . . . | 1320 W (with 125 % margin on available solar array area) |
| Onboard data storage . . . . | 4.6 Tb (3 days of compressed data, enabling retransmission) |
| Survey implementation . . . | Instrument on spin table |
| Attitude control . . . . . | Zero-momentum 3-axis stabilized |

PICO has a single science observing mode, surveying the sky continuously for 5 years using a pre-planned repetitive survey pattern (§ 4.1.2). Instrument data are compressed and stored onboard, then returned to Earth in daily 4-hr Ka-band science downlink passes (concurrent with science observations). Because PICO is observing relatively static Galactic, extragalactic, and cosmological targets, there are no requirements for time-critical observations or data latency. Presently, there are no plans for targets of opportunity or guest observer programs during the prime mission. The PICO instrument does not require cryogenic consumables (as the *Planck* mission did), permitting consideration of significant mission extension beyond the prime mission.

### 4.1.1 Mission Design and Launch

PICO performs its science survey from a quasi-halo orbit around the Earth–Sun L2 Lagrange point. Predecessor missions *Planck* and *WMAP* both operated in L2 orbits.

L2 orbits provide favorable survey geometry (relative to Earth orbits) by mitigating viewing restrictions imposed by terrestrial and lunar stray light. The PICO orbit around L2 is small enough to ensure that the Sun–Probe–Earth (SPE) angle is less than 15°. This maintains the telescope boresight > 70° away from the Earth (Fig. 4.2, $70° = 180° - \alpha - \beta - \text{SPE}$).

High data-rate downlink to the Deep Space Network (DSN) is available from L2 using near-Earth Ka bands. L2 provides a stable thermal environment, simplifying thermal control. The PICO orbit exhibits no post-launch eclipses.

NASA requires that Probes be compatible with an Evolved Expendable Launch Vehicle (EELV). For the purpose of this study, the Falcon 9 [279] is used as the reference vehicle. Figure 4.1 shows PICO configured

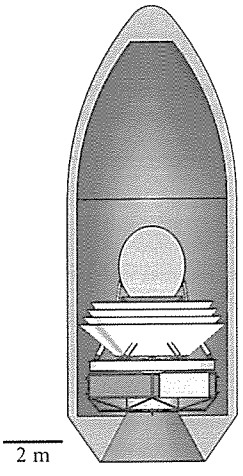


Figure 4.1: PICO is compatible with the Falcon 9.

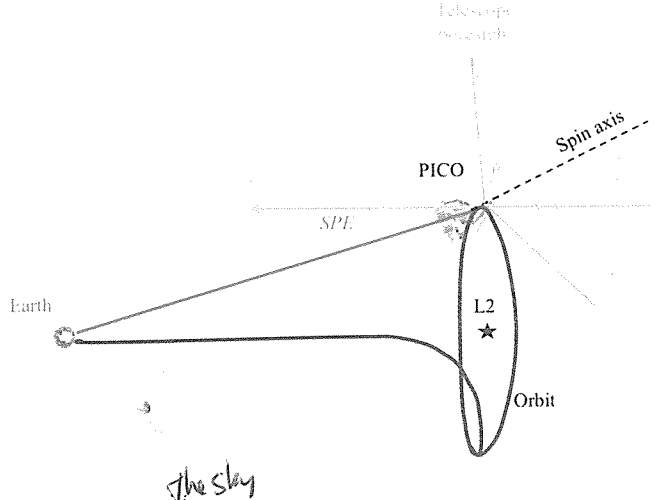


Figure 4.2: PICO surveys the sky by continuously spinning the instrument about a precessing axis.

for launch in a Falcon 9 fairing. The Falcon 9 launch capability for ocean recovery exceeds PICO's 2147 kg total launch mass (including contingency) by a $\sim 50\,\%$ margin.

Insertion to the halo manifold and associated trajectory correction maneuvers (TCMs) require $150\,\mathrm{m\,s^{-1}}$ of total $\Delta V$ by the spacecraft. Orbit maintenance requires minimal propellant (statistical $\Delta V \sim 2\,\mathrm{m\,s^{-1}\,year^{-1}}$). The orbital period is $\sim 6$ months. There are no disposal requirements for L2 orbits, but spacecraft are customarily decommissioned to heliocentric orbit.

### 4.1.2 Survey Design

PICO employs a highly repetitive scan strategy to map the full sky. During the survey, PICO spins with a period $T_{\rm spin} = 1$ min about a spin axis oriented $\alpha = 26°$ from the anti-solar direction (Fig. 4.2). This spin axis is forced to precess about the anti-solar direction with a period $T_{\rm prec} = 10$ hr. The telescope boresight is oriented at an angle $\beta = 69°$ away from the spin axis (Fig. 3.1). This $\beta$ angle is chosen such that $\alpha+\beta > 90°$, enabling mapping of all ecliptic latitudes. The precession axis tracks with the Earth in its yearly orbit around the Sun, so this scan strategy maps the full sky (all ecliptic longitudes) within 6 months.

PICO's $\alpha = 26°$ is chosen to be substantially larger than the *Planck* mission's $\alpha$ angle (7.5°) to mitigate systematic effects by scanning across each sky pixel with a greater diversity of orientations [280]. Increasing $\alpha$ further would decrease the sun-shadowed volume available for the optics and consequently reduce the telescope aperture size. A deployable sun shade was considered, but found not to be required, and was thus excluded in favor of a more conservative and less costly approach.

The instrument spin rate, selected through a trade study, matches that of the *Planck* mission. The study balanced low-frequency ($1/f$) noise subtraction (improves with spin rate) against implementation cost and heritage, pointing reconstruction ability (anti-correlated with spin rate), and data volume (linearly correlated with spin rate). The CMB dipole appears in the PICO data timestream at the spin frequency (1 rpm = 16.7 mHz). Higher multipole signals appear at harmonics of the spin frequency, starting at 33 mHz, above the knee in the detector low-frequency noise (§ 3.2.3). A destriping mapmaker applied in data post-processing effectively operates as a high-pass filter, as demonstrated by *Planck* [281]. PICO's spin-axis precession frequency is $\gg 400\times$ faster than that of *Planck*, greatly reducing the effects of any residual $1/f$ noise by spreading the effects more isotropically across pixels.

## 4.2 Ground Segment

The PICO Mission Operations System (MOS) and Ground Data System (GDS) can be built with extensive reuse of standard tools. The PICO concept of operations is described in § 4.1. All space-ground communications, ranging, and tracking are performed by the Deep Space Network (DSN) 34-m Beam Wave Guide (BWG). X-band is used to transmit spacecraft commanding, return engineering data, and provide navigation information (S-band is a viable alternative, and could be considered in a future trade). Ka-band is used for high-rate return of science data. The baseline 150 Mb/s transfer rate (130 Mb/s information rate after CCSDS encoding) is an existing DSN catalog service [282]. The instrument produces 6.1 Tb/day, which is compressed to 1.5 Tb/day (§ 3.3). Daily 4-hr DSN passes return PICO data in 3.1 hr, with the remaining 0.9 hr available as needed for retransmission or missed-pass recovery.

## 4.3 Spacecraft

The PICO spacecraft bus is Class B and designed for a minimum lifetime of 5 years in the L2 environment. Mission-critical elements are redundant. Flight spares, engineering models, and prototypes appropriate to Class B are budgeted.

The aft end of the spacecraft (the "de-spun module") is comprised of six equipment bays that house standard components (Fig. 4.3). The instrument and V-grooves are mounted on bipods from the spacecraft "spun module," which contains hosted instrument elements (Fig. 3.1). A motor drives the spun module at 1 rpm to support the science survey requirements (§ 4.1.2). Reaction wheels on the despun module cancel the angular momentum of the spun module and provide three-axis control (§ 4.3.1).

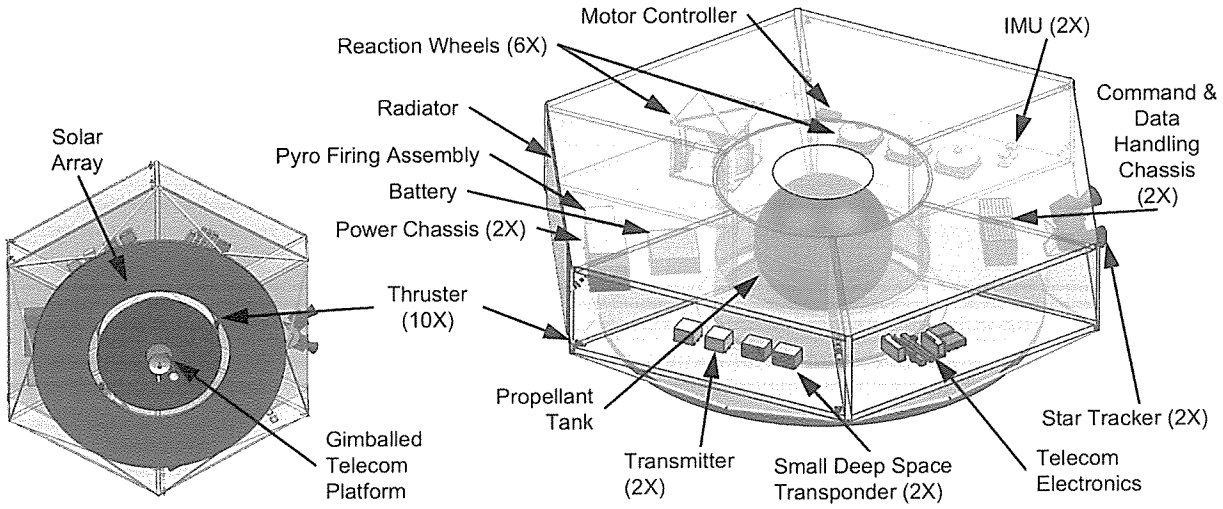


Figure 4.3: Modular equipment bays provide easy access to all components in the spacecraft de-spun module and enable parallel integration of spacecraft subsystems.

The bipods that mechanically support the instrument are thermally insulating. The passively radiating V-groove assembly thermally isolates the instrument from solar radiation and from the bus (§ 3.4.3). Like *Planck* [278], the V-grooves are manufactured using honeycomb material. Additional radiators on the spun and despun spacecraft modules ($\sim 1\,\mathrm{m}^2$ each) reject heat dissipated by spacecraft subsystems and hosted instrument elements.

PICO's avionics are dual-string with standard interfaces. Solid-state recorders provide three days of science data storage (4.6 Tbit), enabling retransmission of missed data.

PICO employs a fully redundant Ka- and X-band telecommunications architecture. The Ka-band system uses a 0.3-m high-gain antenna to support a science data downlink information rate of 130 Mb/s to a 34-m BWG DSN ground station with a link margin of 4.8 dB. The X-band system provides command and engineering telemetry communication through all mission phases using medium- and low-gain antennas. Amplifiers, switches, and all three antennas are on a gimballed platform, enabling Ka and X-band downlink concurrent with science observations.

The heritage power electronics are dual-string. A 74 A-hr Li-ion battery is sized for a 3-hr launch phase with 44 % depth of discharge. After the launch phase, the driving mode is telecom concurrent with science survey (1320 W including 43 % contingency). Solar cells on the aft side of the bus ($5.8\,\mathrm{m}^2$ array, $\alpha = 26°$ off-Sun) support this mode with positive power, and unused area in the solar array plane ($7.4\,\mathrm{m}^2$ more area by growing to 4.5-m diameter) affords 125 % margin (Fig. 4.3).

The propulsion design is a simple mono-propellant blow-down hydrazine system with standard redundancy. Two aft-pointed 22 N thrusters provide $\Delta V$ and attitude control for orbit insertion and maintenance (§ 4.1.1), requiring 140 kg of propellant. Eight 4-N thrusters provide reaction-wheel momentum management and backup attitude-control authority (60 kg of propellant). Accounting for ullage (14 kg), the baseline propellant tank fill fraction is 77 %.

### 4.3.1 Attitude Determination and Control

PICO uses a zero net angular momentum control architecture with heritage from the SMAP mission (§ 6.3). PICO's instrument spin rate (1 rpm) matches that of the *Planck* mission, but the precession of the spin axis is much faster (10 hr vs 6 months), and the precession angle much larger (26° vs 7.5°). These differences make the spin-stabilized *Planck* control architecture impractical because of the amount of torque that would be required to drive precession.

The PICO 1-rpm instrument spin rate is achieved and maintained using a spin motor. The spin-motor drive electronics provide the coarse spin-rate knowledge used for controlling the spin rate to meet the $\pm 0.1$ rpm requirement. Data and power are passed across the interface using slip rings.

Based on mass properties derived from the PICO CAD model, PICO requires 220 N m s to cancel the angular momentum of the instrument and spacecraft spun module (including mass contingency) at 1 rpm. Three Honeywell HR-16 reaction wheel assemblies (RWAs), each capable of 150 N m s, are mounted on the despun module parallel to the instrument spin axis, and spin opposite to the instrument to achieve zero net angular momentum. The despun module is three-axis stabilized. The spin axis is precessed using three RWAs mounted normal to the spin axis in a triangle configuration. Each set of three RWAs is sized such that two could perform the required function with margin, providing single fault tolerance.

Spin-axis pointing and spin-rate knowledge are achieved and maintained using star tracker and inertial measurement unit (IMU) data. The attitude determination system is single-fault tolerant, with two IMUs each on the spun and despun modules, and two star trackers each on the spun and despun modules. Two sun sensors on the despun module are used for safe-mode contingencies and instrument Sun avoidance. All attitude control and reconstruction requirements are met, including spin axis control $< 60$ arcmin with $< 1$ arcmin/min stability, and reconstructed pointing knowledge $< 10$ arcsec (each axis, $3\sigma$).

Additional pointing reconstruction is performed in post-processing using the science data. The PICO instrument will observe planets (compact, bright sources) nearly every day. By fitting the telescope pointing to the known planetary ephemerides, the knowledge of the telescope boresight pointing and the relative pointing of each detector will improve to better than 1 arcsec (each axis, $3\sigma$). *Planck*, with fewer detectors, making lower signal-to-noise ratio measurements of the planets, and observing with a scan strategy that acquired measurements of each planet only once every 6 months, demonstrated 0.8 arcsec ($1\sigma$) pointing reconstruction uncertainty in-scan and 1.9 arcsec ($1\sigma$) cross-scan [283].

# 5 Technology Maturation

PICO builds off of the heritage of *Planck*-HFI and *Herschel*. Since *Planck* and *Herschel*, suborbital experiments have used monolithically fabricated TES bolometers and multiplexing schemes to field instruments with thousands of TES bolometers per camera (Fig. 5.1). By the time PICO enters Phase A, the Simons Observatory plans to be operating 60,000 TES bolometers [284].

The remaining technology developments required to enable the PICO baseline design are:

1. Extension of three-color antenna-coupled bolometers down to 21 GHz and up to 462 GHz (§ 5.1);
2. Construction of high-frequency direct absorbing arrays and laboratory testing (§ 5.2);
3. Beam line and 100-mK testing to simulate the cosmic ray environment at L2 (§ 5.3);
4. Expansion of time-division multiplexing to support 128 switched rows per readout column (§ 5.4).

All of these developments are straightforward extensions of technologies already available today. We recommend APRA and SAT support to complete development of these technologies through the milestones described in Table 5.1.

## 5.1 21–462 GHz Bands

Suborbital teams have successfully demonstrated a variety of optical-coupling schemes, including horns with ortho-mode transducers (OMTs), lithographed antenna arrays, and sinuous antennas under lenslets (Table 5.2). All have achieved background-limited performance in suborbital instruments with sufficient margin on design parameters to achieve this performance in the lower background environment at L2. All have been packaged into modules and focal-plane units in working cameras representative of the PICO integration. Experiments have covered many of PICO's observing bands between 27 GHz and 270 GHz (Table 5.2). To date, suborbital experiments have achieved statistical map depths of 3 $\mu K_{CMB}$ arcmin on degree-scaled modes over small parts of the sky, within an order of magnitude of what PICO achieves

Table 5.1: PICO technologies can be developed to TRL 5 prior to a 2023 Phase A start using the APRA and SAT programs, requiring a total of about $ 13M. Per NASA guidance, these costs are outside the mission cost (§ 6.5).

| Task | Current status | Milestone A | Milestone B | Milestone C | Current funding | Required funding | Date TRL5 achieved |
|---|---|---|---|---|---|---|---|
| 1a. Three-color arrays $\nu < 90$ GHz | 2-color lab demos $\nu > 30$ GHz | Field demo of 30–40 GHz (2020) | Lab demos 20–90 GHz (2022) | — | APRA & SAT funds | $2.5M over 4 yr (1 APRA + 1 SAT) | 2022 |
| 1b. Three-color arrays $\nu > 220$ GHz | 2-color lab demos $\nu < 300$ GHz | Field demo of 150–270 GHz (2021) | Lab demos 150-460 GHz (2022) | — | APRA & SAT funds | $3.5M over 4 yr (2 SATs) | 2022 |
| 2. Direct absorbing arrays $\nu > 50$ GHz | 0.1–5 THz unpolarized | Design and prototype of arrays (2021) | Lab demo of 555 GHz (2022) | Lab demo of 799 GHz (2023) | None | $2M over 5 yr (1 SAT) | 2023 |
| 3. Cosmic ray studies | 250 mK w/ sources | 100 mK tests with sources (2021) | Beamline tests (2023) | — | APRA & SAT funds | $0.5–1M over 5 yr (part of 1 SAT) | — |
| 4a. Fast readout electronics | MUX66 demo | Engineering and Fab of electronics (2020) | Lab demo (2021) | Field demo (2023) | No direct funds | $4M over 5 yr (1 SAT) | 2023 |
| 4b. System engineering; 128× MUX demo | MUX66 demo | Design of cables (2020) | Lab demo (2021) | Field demo (2023) | No direct funds | | |

over the entire sky (Table 3.2), and have demonstrated systematic control better than this level through full-pipeline simulations and null-test analysis (jackknife tests).

The baseline PICO instrument requires three-color dual-polarized antenna-coupled bolometers covering bands from 21 to 462 GHz (§ 3.2.1). The sinuous antenna has the bandwidth to service three bands per pixel, whereas horns and antenna arrays have only been used for two. Our baseline is to use a three-band sinuous antenna, although we have a design for PICO that uses two-bands per pixel and has the same baseline noise as PICO (§ 5.5). SPT-3G has used the PICO-baselined three-color pixel design to deploy 16,000 detectors covering 90/150/220 GHz [285].

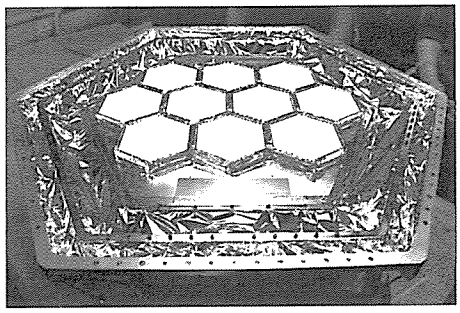

Figure 5.1: SPT-3G operates a focal plane with sinuous antenna-coupled, three-band pixels with 16,000 bolometers [285]. Each pixel couples radiation to bands at 95, 150, and 220 GHz.

The extension to lower frequencies requires larger antennas and therefore control of film properties and lithography over larger areas. Scaling to higher frequencies requires tighter fabrication tolerances and materials tend to exhibit higher losses. Current anti-reflection technologies for the lenslets need to be extended with thicker and thinner layers to cover the lowest and highest frequency channels. These developments will require tight control of cleanliness and understanding of process parameters. All developments require careful characterization of beam properties.

The direction of polarization sensitivity of the sinuous antenna varies with frequency. Over 25% bandwidth, the variation is approximately ±5 deg [289]. There are potential solutions to this in

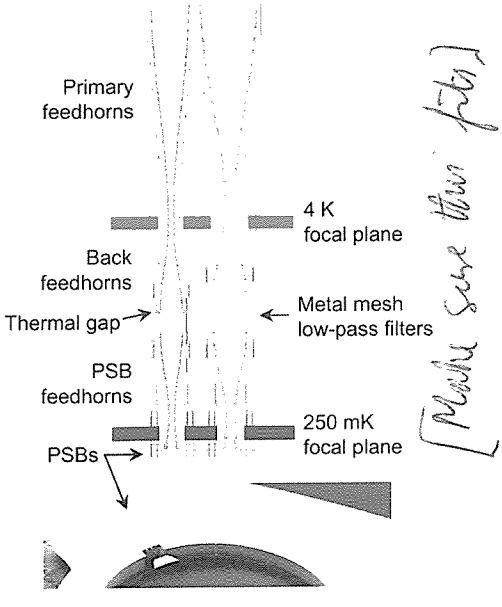

Table 5.2: Multiple active suborbital efforts are advancing technologies relevant to PICO.

| Project | Type | Optical Coupling | $\nu_c$ [GHz] | Colors per pixel | $N_{\rm bolo}$ | Significance | Reference |
|---|---|---|---|---|---|---|---|
| PICO baseline . . . . . | Flight | | 21 – 462 | Three | 11,796 | | § 3.2.1 |
| SPT-3G . . . . . | Ground | Sinuous | 90 – 220 | Three | 16,260 | Trichroic | [285] |
| Advanced ACT-pol . . . | Ground | Horns | 27 – 230 | Two | 3,072 | Dichroic | [286] |
| BICEP/Keck . . . . . | Ground | Antenna arrays | 90 – 270 | One | 5,120 | 50 nK-deg | [32] |
| Berkeley, Caltech, NIST | Lab | Various | 30 – 270 | Various | – | Band coverage | [260, 287, 288] |
| SPIDER . . . . . | Balloon | Antenna arrays | 90 – 150 | One | 2,400 | Stable to 10 mHz | [258] |

Table 5.3: PICO high-frequency detectors leverage development and demonstration by *Planck*, *Herschel*, and SPT.

| Project | Type | Polarized | Mono-lithic? | $\nu_c$ [GHz] | Colors per pixel | $N_{\rm bolo}$ | Significance | Reference |
|---|---|---|---|---|---|---|---|---|
| PICO baseline . . . . . | Flight | Yes | Yes | 555 – 799 | One | 1,200 | | § 3.2.2 |
| *Planck* HFI . . . . . | Flight | 143–343 GHz | No | 143 – 857 | One | 48 | TRL 9 polarized | [256] |
| *Herschel* . . . . . | Flight | No | Yes | 570 – 1200 | One | 270 | TRL 9 monolothic | [292] |
| SPT-SZ . . . . . | Ground | No | Yes | 90 – 220 | One | 840 | Monolithic array TESs | [254] |
| SPT-pol-90 . . . . . | Ground | Yes | No | 90 | One | 180 | Dual pol absorbing TESs | [293] |

the focal plane design, measurements, data analysis, and free parameters of the antenna geometry. A recent study found that pre-flight characterization of the effect through measurements can readily mitigate this ~~systematic~~ effect [290]. Systematic effect studies for current field demonstrations, such as with the data of SPT-3G, will be particularly important. The PICO concept is robust to any challenges in developing three-color pixels; § 5.5 describes an option to descope to two-color horn-coupled pixels, a technology with which the polarization sensitivity is constant as a function of frequency.

## 5.2 555–799 GHz bands

The baseline PICO instrument requires single-color, horn-coupled, dual-polarization, direct-absorbing bolometers from 555 to 799 GHz (§ 3.2.2). *Planck* and *Herschel* demonstrated the architecture of horns coupled to direct absorbing bolometers (Fig. 5.2). Ground experiments with similar designs have deployed focal planes with hundreds of horn-coupled spiderweb bolometers, replacing the *Planck* and *Herschel* NTD-Ge thermistors with TESs, and adjusting time constants as necessary (Table 5.3). *Planck*-HFI, SPT-pol, and BICEP demonstrated dual-polarized detectors. *Herschel* and SPT-SZ demonstrated monolithic unpolarized detectors. PICO will require detectors that merge these two designs in monolithic dual-polarized arrays. Since all the components of the technology already exist, the remaining necessary development is the packaging. Filled arrays of detectors such as Backshort Under Ground (BUG) bolometers are also an option [291].

## 5.3 Environmental Testing

Laboratory tests and in-flight data from balloons suggest that TES bolometer arrays may be more naturally robust against cosmic rays than the individual NTD-Ge bolometers used in *Planck*. PICO will leverage lessons learned from *Planck* and ensure robust thermal sinking of detector array substrates. Cosmic-ray glitches have fast recovery times and low coincidence rates [294, 295]. Residual risk can be retired with

100 mK testing where the array heat sinking may be weaker, and beam-line tests to simulate the expected flight environment.

## 5.4 Multiplexing

More than ten experiments have used time-domain multiplexer (TDM) readout. SCUBA2 on JCMT has 10,000 pixels, nearly as many detectors as planned for PICO [296]. Most of these experiments have used 32-row multiplexing. Recently ACT has expanded this to 64-row multiplexing [259].

PICO's sensitivity requirements dictate the use of 13,000 transition-edge-sensor bolometers, requiring a highly multiplexed system. The PICO baseline design calls for TDM with 128 switched rows per readout column (TDM-128×). The leap to TDM-128× requires:

- development of fast-switched room temperature electronics; and
- system engineering of room temperature to cryogenic row select cabling to ensure sufficiently fast row switch settling times.

The historical row revisit rate for bolometric instruments using 32× TDM has been 25 kHz [e.g., 250]. However, X-ray instruments using TDM routinely switch between rows at a rate of 160 ns [297]. The PICO baseline assumes a 160 ns switch rate and TDM-128×, which dictates a row revisit rate (effective sampling rate) of 48.8 kHz. To limit aliased noise, PICO implements L/R filters in each readout channel with a bandwidth of 6 kHz, dictated by detector stability considerations and the required $\sim$ 1 kHz signal bandwidth. With these parameters and using the same TDM multiplexer SQUID design, the increased total noise due to aliasing will be limited to 15 %. The system engineering study will culminate in a demonstration of TDM-128× SQUID aliased noise below PICO detector sensitivity requirements.

## 5.5 Technology Descopes

A descope from three-color sinuous antenna/lenslet-coupled pixels to two-color horn-coupled pixels remains a viable alternative should the three-color technology not mature as planned. Descope studies suggest that a PICO-size focal plane using two-color horn-coupled pixels at the lower frequencies and the baseline one-color pixels at the higher frequencies would contain 8,840 detectors (compared to the baseline 12,966) and map in 19 colors (baseline 21). Because horns have a 2.3 : 1 bandwidth, each of the two bands in a pixel has 35 % bandwidth (compared to the baseline 25 %), which compensates for pixel count, resulting in 0.61 $\mu K_{CMB}$-arcmin aggregate CBE map depth, which matches the PICO CBE map depth, and affords $> 40$ % margin against the 0.87 $\mu K_{CMB}$-arcmin baseline requirement (Table 3.2), but with coarser spectral resolution. Detailed analysis could be performed to assess the impact on signal component separation (§ 2.7).

## 5.6 Enhancing Technologies

The following technologies are neither required nor assumed by the PICO baseline concept. They represent opportunities to extend scientific capabilities or simplify engineering.

PICO baselines TDM readout because of its relative maturity and demonstrated sensitivity and stability in relevant science missions. Lab tests of frequency-domain multiplexing (FDM) suggest comparable performance with higher multiplexing factors and lower loads on cryogenic stages relative to TDM. Suborbital experiments such as SPT-3G have used frequency-division multiplexing (FDM) to readout focal planes comparable in size to PICO.

Microwave frequency SQUID multiplexing can increase the multiplexing density and reduce the number of lines between the 4 K and ambient temperature stages [298, 299]. Kinetic inductance detectors (KIDs) and thermal KIDs (TKIDs) can further reduce the wire count, obviate the SQUIDs, and dramatically simplify integration by performing multiplexing on the same substrate as the detectors themselves [300–302]. The cost to develop these technologies is $3–4M/year, with a high chance of reaching TRL-5 before Phase A.

# 6 Project Management, Heritage, Risk, and Cost

## 6.1 PICO Study Participants

The PICO study was open to the entire mm/sub-mm science community. Seven working groups were led by members of PICO's Executive Committee, which met weekly under the leadership of PI Shaul Hanany. More than 60 people participated in-person in two community workshops (November 2017 and May 2018).

The PICO engineering concept definition package was generated by Team X (the JPL concurrent design lab). The Team X study was supported by inputs from a JPL engineering team and Lockheed Martin.

The full list of study report contributors and endorsers is on page i.

## 6.2 Project Management Plan

PICO benefits from the experience of predecessor missions such as *Planck* and *WMAP*, as well as many years of investment in technology development and a multitude of suborbital experiments. In addition to demonstrated science and engineering capabilities, this heritage has developed a community of people with the expertise required to field a successful mission.

This study assumes mission management by JPL with a Principal Investigator leading a single science team. A Project Manager provides project oversight for schedule, budget, and deliverables. A Project Systems Engineer leads systems engineering activities and serves as the Engineering Technical Authority. A Mission Assurance Manager serves as the Independent Technical Authority. The PICO mission development schedule is shown in Fig. 6.1.

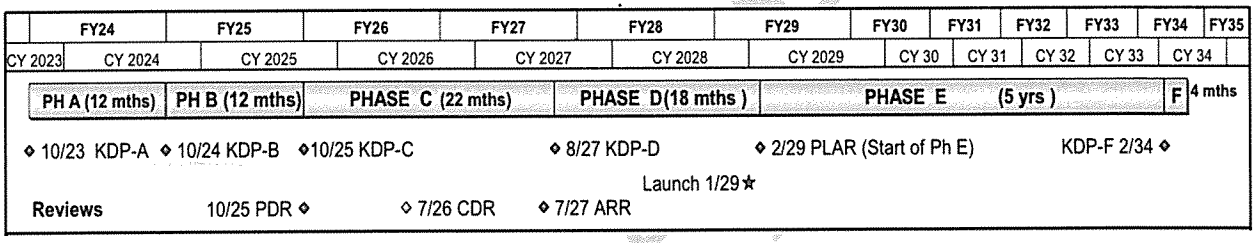


Figure 6.1: The PICO baseline schedule is based on historical actuals from similarly-sized missions such as Juno and SMAP. Per NASA direction, Probe studies assume a Phase A start in October 2023.

Probes are medium-class missions, similar in cost scope to NASA's New Frontiers missions, which are Category 1 and Risk Classification A or B, with Phase A–D costs capped at ~~$~~ $850M (not including the launch vehicle). JPL is well-prepared to manage Probe missions, having managed the Juno New Frontiers mission (launched 2011) and also the development of the medium-class *Spitzer* Space Telescope (launched 2003). JPL delivered the bolometric detectors for the *Planck* HFI instrument (launched 2009). Presently, JPL is managing NEOCam, a Discovery class infrared space telescope.

The PICO spacecraft provider will be selected during mission formulation. Multiple organizations are capable of providing a spacecraft bus to meet PICO's requirements. Lockheed Martin contributed to the PICO concept study, leveraging their experience with New Frontiers missions Juno and OSIRIS-REx.

## 6.3 Heritage

The successful *Planck* mission provides science heritage for PICO. Technical heritage traces to multiple missions.

Because PICO observes in the mm/sub-mm regime, the surface accuracy requirement for the reflectors is relatively easy to meet. PICO's reflectors are similar to *Planck*'s, but somewhat larger (270 cm × 205 cm primary vs. 189 cm × 155 cm) [303]. *Herschel* observed at wavelengths more demanding than PICO's and was larger (350 cm diameter primary) [304].

The heritage of the PICO detectors and readout electronics (§ 3.2, § 3.3) is described in § 5.

PICO's detectors are cooled by a cADR (§ 3.4.1) with requirements that are within the capabilities of current ADRs developed by Goddard Space Flight Center. These systems have been applied to several

JAXA missions, including *Hitomi* [272].

PICO's 4 K cryocooler (§ 3.4.2) is a direct extension of the JWST MIRI design [273, 274]. PICO benefits from a simpler and more reliable implementation of the J-T system than was required for MIRI, in that no deployment of cooling lines is required, and all flow valving is performed on the warm spacecraft. Cooling multiple independent points with a J-T loop has been demonstrated on *Planck* with the JPL-supplied 18 K cooler [305].

Structures similar to PICO's V-groove radiator assembly (§ 3.4.3) are a standard approach for passive cooling, first described more than thirty years ago [306]. PICO has baselined a simple honeycomb material construction like that successfully flown by the *Planck* mission [305, 307].

Most requirements on the PICO spacecraft are well within typical ranges and can be met with standard high-heritage systems (§ 4.3). PICO's spin-architecture and data-volume requirements are less typical, and discussed below.

PICO's spin system is generally less demanding than the successful SMAP spin system. PICO spins its instrument at 1 rpm, passes data and power across the spin interface (Fig. 3.2), and requires ≈ 220 N m s of spin momentum cancellation (§ 4.3.1). SMAP spins its 6-m instrument antenna at 14.6 rpm, successfully passes data and power across the spin interface, and requires 359 N m s of spin momentum cancellation [308].

Though PICO's data volume is notable by current standards, it is already enveloped by missions in development. PICO produces 6.1 Tb/day of raw data, which is compressed to 1.5 Tb/day (§ 3.3). PICO downlinks data daily, but baselines storage of 3 days of (compressed) data to mitigate missed telecom passes. This requires 4.5 Tb of onboard storage, in family with the 3.14 Tb solid-state recorder currently in use by Landsat 8 and much smaller than the 12 Tb flash memory planned for NISAR [309]. The PICO baseline 150 Mb/s Ka-band data downlink is an existing DSN catalog service [282]. The baseline PICO mission generates ≈ 2,200 Tb of raw (uncompressed) data per year, less than the ≈ 6,800 Tb/year currently returned by Landsat 8 and ≈ 9,300 Tb/yr planned by NISAR [309].

## 6.4 Risk Assessment

### 6.4.1 Pre-Mission Risks

Technology development (§ 5) is performed prior to the beginning of mission development, and is outside of the mission cost (per NASA direction), so associated risks do not represent threats to the cost of mission development. Rather, these technology development risks affect the availability of the described baseline mission. A technology-related mission descope is described in § 5.5.

### 6.4.2 Development Risks

PICO's healthy contingencies, margins, and reserves provide flexibility to address risks realized during mission development. PICO carries > 40 % instrument sensitivity margin (Table 3.2), > 100 % heat lift margin (Table 3.3), 43 % system power contingency, 31 % payload mass contingency, and 25 % spacecraft mass contingency. The Falcon 9 launch capability (assuming ocean recovery) exceeds PICO's total launch mass (including contingency) by a ∼ 50 % margin. The PICO budget includes 30 % cost reserves for Phases A–D (§ 6.5).

During mission development the Project Systems Engineer continually assesses risks, tracks progress toward retiring them, and updates mitigations. Mitigations for a few top risks identified during this study are described below.

- Thermal risk can be mitigated through extensive thermal modeling and review in Phase A, and design for early test verification.
- Risks associated with the instrument spin architecture can be mitigated by engaging JPL engineers who were involved in the SMAP mission.
- Detector delivery schedule risk can be mitigated by beginning fabrication early in the project life cycle

and fabricating a generous number of detector wafers to ensure adequate yield. Multiple institutions (including, for example, JPL, GSFC, NIST, and ANL) would be capable of producing the PICO detectors. Suborbital programs generally achieve > 66 % detector wafer yield.

- Risks associated with the integration and test of a cryogenic instrument can be mitigated through advanced planning and allocation of appropriate schedule and schedule margin.

### 6.4.3 Operations Risks

The PICO design meets the requirements associated with the NASA Class B risk classification. For Class B missions, essential spacecraft and instrument functions are typically fully redundant. This increases mission cost, but significantly reduces the risk of mission failure.

The PICO mission utilizes a single instrument with a single observing mode mapping the sky using a repetitive survey pattern. The mission does not require any time-critical activities. The observatory fits in to the launch vehicle fairing in its operational configuration, so no hardware deployments are required. Because PICO observes at long wavelengths, the telescope does not require a dust cover (nor the associated mission-critical cover release).

The spacecraft incorporates a fault protection system for anomaly detection and resolution. The Sun-pointed, command receptive, thermally stable safe-mode attitude allows ground intervention for fault resolution without time constraints. PICO's high degree of hardware redundancy and onboard fault protection ensure spacecraft safety in the event of unforeseen failures and faults.

As described in § 2.7 and § 2.8, pre-Phase A simulation software maturation is recommended to mitigate the challenges associated with foreground separation and systematics control.

## 6.5 Mission Cost

We estimate PICO's total Phase A–E lifecycle cost between $870M and $960M, including the $150M allocation for the Launch Vehicle (per NASA direction). These cost estimates include 30 % reserves for development (Phases A–D) and 13 % reserves for operations (Phase E). Pre-Phase-A technology maturation (§ 5) will be accomplished through the normal APRA and SAT processes, and is not included in the mission cost (per NASA direction).

Table ?? shows the mission cost breakdown, including the JPL Team X cost estimate as well as the PICO team cost estimate. Team X is JPL's concurrent design facility. Team X estimates are generally model-based, and were generated after a series of instrument and mission-level studies. Their accuracy is commensurate with the level of understanding typical to Pre-Phase-A concept development. They do not constitute an implementation or cost commitment on the part of JPL or Caltech.

The PICO team has generally adopted the Team X estimates, but also obtained a parametrically estimated cost range for the Flight System (WBS 6) and Assembly, Test, and Launch Operations (ATLO, WBS 7) from Lockheed Martin Corporation to represent the cost benefits that might be realized by working with an industry partner. After adding estimated JPL overhead and Team X estimated V-groove assembly costs (not included in the Lockheed estimate), the PICO team cost is in-family with but lower than the Team X cost (Table ??).

Management, Systems Engineering, and Mission Assurance (WBS 1–3) development costs scale linearly with the WBS 4–12 development costs in the Team X model, and are adjusted accordingly in the PICO team estimate. Science team (WBS 4) costs are assessed by Team X based on PICO science team estimates of the numbers and types of contributors and meetings required for each year of PICO mission development and operations. These workforce estimates are informed by recent experience with the *Planck* mission.

Payload system (WBS 5) costs are discussed in detail in § 6.5.1. PICO's spacecraft (WBS 6) cost reflects a robust Class B architecture (§ 4.3). Mission-critical elements are redundant. Appropriate flight spares, engineering models and prototypes are budgeted. The V-groove assembly (§ 3.4.3) is costed in WBS 6. Mission operations (WBS 7), Ground Data Systems (WBS 9), and Mission Navigation and Design (WBS 12)

costs reflect a relatively simple concept of operations (§ 4.1). PICO has a single instrument with a single science observing mode, surveying the sky continuously using a pre-planned repetitive survey pattern. Orbit maintenance activities are simple and infrequent.

### 6.5.1 Payload Cost

The PICO payload consists of a single instrument: an imaging polarimeter. Payload costs are tabulated in Table 6.2.

Table 6.2: Detailed breakdown of PICO instrument costs.

| Instrument Elements | Cost |
|---|---|
| Management, Systems Eng., Assurance | $ 18M |
| 4 K Cooler and 0.1 K cADR | $ 71M |
| Focal plane and electronics | $ 27M |
| Mechanical, Thermal, Software | $ 17M |
| Telescope | $ 6M |
| Instrument integration and test | $ 29M |
| Total Instrument Cost | $ 168M |

The superconducting detectors require sub-kelvin cooling to operate. The active cooling system (the 0.1 K cADR and 4 K cryocooler, § 3.4.1 and § 3.4.2) comprises nearly half of the payload cost. The cADR cost for this study is an estimate from NASA Goddard Space Flight Center (GSFC), and assumes the provision of both a flight model and an engineering model. GSFC has produced ADRs for multiple spaceflight missions. The 4 K cryocooler cost for this study is based on the NASA Instrument Cost Model (NICM) VIII CER Cryocooler model [310], assuming a commercial build. PICO benefits greatly from recent and ongoing investment by commercial suppliers of 4 K coolers (as described in § 3.4.2). Team X used NICM VIII to model the cost of the focal plane and dual-string readout electronics (§ 3.2, § 3.3). Team X estimated the telescope cost using the Stahl model [311]. The telescope is not a major cost driver, primarily because the reflectors only need to be diffraction limited at 330 $\mu$m (900 GHz) (§ 3.1).

Based on JPL experience, 18 % of the instrument cost is allocated for integration and test. This includes integration and test of the flight focal-plane assembly with the flight cADR and then integration and test of the complete instrument including the focal-plane assembly, reflectors, structures, and coolers (§ 3.5). Integration and test of the instrument with the spacecraft is costed in WBS 10 (ATLO).

# NASA Standard Template Cost Table

## 2020 Astrophysical Decadal Survey - Probe Mission Preparatory Study
## Master Equipment List Based Parametric Total Lifecycle Cost Estimate

***Mission Name / Acronym:*** **PICO**

***Cost Estimator:*** JPL Team X

***Date of Cost Estimate:*** October 9, 2018

***Cost Estimate Based On:*** Final Master Equipment List

| ***PROJECT PHASE*** | | ***COST [FY18 $M]*** |
|---|---|---|
| **Phase A** | | (see Note 1) |
| **Phases B-D** | Mgmt, SE, MA | $54 |
| | Science | $19 |
| | Telescope | $6 |
| | Instrument | $162 |
| | Spacecraft, including ATLO | $272 |
| | MOS/GDS | $44 |
| | Launch Vehicle and Services | $150 |
| | Reserves | $167 |
| | ***Total Cost Phases B-D*** | ***$874*** |
| **Phase E-F** | Operations | $74 |
| | Reserves | $10 |
| | ***Total Cost Phases E-F*** | **$84** |
| | **TOTAL LIFECYCLE COST** | **$958** |

***Notes:***

*- Team X estimates costs for Phase A-D. A break out of Phase A cost is not available. In this table, Phase A costs are included in Phase B-D.*

*- This parametric cost estimate is based on the Probe's Master Equipment List derived from the Final Engineering Concept Definition Package that accurately reflects the mission described in the Probe's Final Report. This estimate is to be used only for non-binding rough order of magnitude planning purposes.*

*- Team X estimates are generally model-based, and were generated after a series of instrument and mission-level studies. Their accuracy is commensurate with the level of understanding typical to Pre-Phase-A concept development. They do not constitute an implementation or cost commitment on the part of JPL or Caltech.*

# References


[1] A. Mennella, M. Bersanelli, R. C. Butler *et al.*, "Planck early results. III. First assessment of the Low Frequency Instrument in-flight performance," *Astron. Astrophys.*, vol. 536, p. A3, Dec. 2011. Retrieved from: http://adsabs.harvard.edu/abs/2011A%26A...536A...3M

[2] Planck HFI Core Team, P. A. R. Ade, N. Aghanim *et al.*, "Planck early results. IV. First assessment of the High Frequency Instrument in-flight performance," *Astron. Astrophys.*, vol. 536, p. A4, Dec. 2011. Retrieved from: http://adsabs.harvard.edu/abs/2011A%26A...536A...4P

[3] N. Jarosik, C. Barnes, C. L. Bennett *et al.*, "First-Year Wilkinson Microwave Anisotropy Probe (WMAP) Observations: On-Orbit Radiometer Characterization," *Ap. J. Suppl.*, vol. 148, pp. 29–37, Sep. 2003. Retrieved from: http://adsabs.harvard.edu/abs/2003ApJS..148...29J

[4] U. Seljak and M. Zaldarriaga, "Signature of Gravity Waves in the Polarization of the Microwave Background," *Physical Review Letters*, vol. 78, pp. 2054–2057, Mar. 1997. Retrieved from: http://adsabs.harvard.edu/abs/1997PhRvL..78.2054S

[5] M. Kamionkowski, A. Kosowsky, and A. Stebbins, "A Probe of Primordial Gravity Waves and Vorticity," *Phys. Rev. Lett.*, vol. 78, pp. 2058–2061, Mar. 1997, astro-ph/9609132. Retrieved from: http://adsabs.harvard.edu/cgi-bin/nph-bib_query?bibcode=1997PhRvL..78.2058K&db_key=AST

[6] M. Zaldarriaga and U. Seljak, "All-sky analysis of polarization in the microwave background," *Phys. Rev. D.*, vol. 55, pp. 1830–1840, Feb. 1997. Retrieved from: http://adsabs.harvard.edu/abs/1997PhRvD..55.1830Z

[7] M. Kamionkowski, A. Kosowsky, and A. Stebbins, "Statistics of cosmic microwave background polarization," *Phys. Rev. D.*, vol. 55, pp. 7368–7388, Jun. 1997. Retrieved from: http://adsabs.harvard.edu/abs/1997PhRvD..55.7368K

[8] S. W. Henderson, R. Allison, J. Austermann *et al.*, "Advanced ACTPol Cryogenic Detector Arrays and Readout," *Journal of Low Temperature Physics*, vol. 184, pp. 772–779, Aug. 2016. Retrieved from: http://adsabs.harvard.edu/abs/2016JLTP..184..772H

[9] B. A. Benson, P. A. R. Ade, Z. Ahmed *et al.*, "SPT-3G: a next-generation cosmic microwave background polarization experiment on the South Pole telescope," in *Society of Photo-Optical Instrumentation Engineers (SPIE) Conference Series*, ser. Society of Photo-Optical Instrumentation Engineers (SPIE) Conference Series, vol. 9153, Jul. 2014, p. 1. Retrieved from: http://adsabs.harvard.edu/abs/2014SPIE.9153E..1PB

[10] N. Galitzki, A. Ali, K. S. Arnold *et al.*, "The Simons Observatory: instrument overview," in *Millimeter, Submillimeter, and Far-Infrared Detectors and Instrumentation for Astronomy IX*, ser. Society of Photo-Optical Instrumentation Engineers (SPIE) Conference Series, vol. 10708, Jul. 2018, p. 1070804. Retrieved from: http://adsabs.harvard.edu/abs/2018SPIE10708E..04G

[11] T. Essinger-Hileman, A. Ali, M. Amiri *et al.*, "CLASS: the cosmology large angular scale surveyor," in *Millimeter, Submillimeter, and Far-Infrared Detectors and Instrumentation for Astronomy VII*, ser. *Proceedings of SPIE*, vol. 9153, Jul. 2014, p. 91531I. Retrieved from: http://adsabs.harvard.edu/abs/2014SPIE.9153E..1IE

[12] H. Hui, P. A. R. Ade, Z. Ahmed *et al.*, "BICEP Array: a multi-frequency degree-scale CMB polarimeter," in *Millimeter, Submillimeter, and Far-Infrared Detectors and Instrumentation for Astronomy IX*, ser. Society of Photo-Optical Instrumentation Engineers (SPIE) Conference Series, vol. 10708, Jul. 2018, p. 1070807. Retrieved from: http://adsabs.harvard.edu/abs/2018SPIE10708E..07H

[13] A. A. Fraisse, P. A. R. Ade, M. Amiri *et al.*, "SPIDER: probing the early Universe with a suborbital polarimeter," *JCAP*, vol. 4, p. 47, Apr. 2013. Retrieved from: http://adsabs.harvard.edu/abs/2013JCAP...04..047F

[14] J. Lazear, P. A. R. Ade, D. Benford *et al.*, "The Primordial Inflation Polarization Explorer (PIPER)," in *Millimeter, Submillimeter, and Far-Infrared Detectors and Instrumentation for Astronomy VII*, ser. *Proceedings of SPIE*, vol. 9153, Jul. 2014, p. 91531L. Retrieved from: http://adsabs.harvard.edu/abs/2014SPIE.9153E..1LL

[15] A. H. Guth, "Inflationary universe: A possible solution to the horizon and flatness problems," *Phys. Rev. D.*, vol. 23, pp. 347–356, Jan. 1981. Retrieved from: http://adsabs.harvard.edu/abs/1981PhRvD..23..347G

[16] A. D. Linde, "A new inflationary universe scenario: A possible solution of the horizon, flatness, homogeneity, isotropy and primordial monopole problems," *Physics Letters B*, vol. 108, pp. 389–393, Feb. 1982. Retrieved from: http://adsabs.harvard.edu/abs/1982PhLB..108..389L

[17] A. Albrecht and P. J. Steinhardt, "Cosmology for grand unified theories with radiatively induced symmetry breaking," *Physical Review Letters*, vol. 48, pp. 1220–1223, Apr. 1982. Retrieved from: http://adsabs.harvard.edu/abs/1982PhRvL..48.1220A

[18] A. A. Starobinsky, "A new type of isotropic cosmological models without singularity," *Physics Letters B*, vol. 91, pp. 99–102, Mar. 1980. Retrieved from: http://adsabs.harvard.edu/abs/1980PhLB...91...99S

[19] V. F. Mukhanov and G. V. Chibisov, "Quantum fluctuations and a nonsingular universe," *Soviet Journal of Experimental and Theoretical Physics Letters*, vol. 33, p. 532, May 1981. Retrieved from: http://adsabs.harvard.edu/abs/1981JETPL..33..532M

[20] A. H. Guth and S. Pi, "Fluctuations in the new inflationary universe," *Phys. Rev. Lett.*, vol. 49, pp. 1110–1113, Oct. 1982. Retrieved from: http://adsabs.harvard.edu/cgi-bin/nph-bib_query?bibcode=1982PhRvL..49.1110G&db_key=AST